Superconductivity of the Kronig-Penney model

Yukio Tanaka and Masaru Tsukada
Department of Physics, Faculty of Science, University of Tokyo, Hongo 7-3-1 Bunkyo-ku, Tokyo, Japan
(Received 16 May 1988; revised manuscript received 20 March 1989)

We clarify the basic properties of superconductivity in the Kronig-Penney model, which mimics a layered superconductor or superconducting superlattice, taking into consideration the electron's motion parallel to the layer. The exact integral kernel of the Gor'kov equation is obtained by the analytical Green's function and based on it a Friedel-type microscopic oscillation of the pair potential at the boundary is correctly treated for the first time. The transition temperature T_c is calculated with a rigorous treatment of the interband effect. It is found that this quantity can only be correctly determined by solving the Gor'kov equation with proper inclusion of the spatial dependence of the pair potential. It cannot be determined only by densities of states obtained from band calculations with the use of a simple BCS equation. The dependence of T_c on the superlattice period and the spatial dependence of the pair potential are also discussed. The critical temperature shows nonmonotonic behavior as a function of the thickness period, which cannot be explained by the usual theory of the proximity effect by de Gennes.

I. INTRODUCTION

With the rapid development of technologies for fabricating artificial materials, it is possible to design superconducting microdevices at the atomic scale,[1-3] and superconducting superlattices[4-11] may become promising candidates for new devices. Novel types of superconducting systems recently developed cannot be adequately described by the existing theories of superconductivity due to many limitations.

There still remain many difficulties and unsolved problems in the theory of superconductivity in spite of its long history. Superconductivity in nonuniform materials is not fully understood on a microscopic basis, for example. There are many phenomena that originate essentially from the lack of uniformity of the system. For example, the superconducting proximity effect[12-19] and the Josephson effect[20-22] are examples of nonuniform superconducting systems, and previous theories for such systems are rather phenomenological and cannot be considered fully microscopic.

Superconducting superlattices are very interesting because they can be designed at the atomic scale. By changing the length of the unit period or choosing the kind of material constructing the periodic structure, we can fabricate many new materials. When its unit period is large, the property of the superconductor–normal-material superlattice is nearly equal to that of the superconductor–normal-material junction. But reducing the length of the unit period, the microscopic wave character becomes significant and would show exotic properties.

Most of the superconducting superlattices produced thus far are dirty because of the atomic diffusion near the interface; so we cannot fully control the character of the superconducting superlattice at our disposal. But in the near future it may be possible to fabricate clean superconducting superlattices by choosing an appropriate combination of materials and method of preparation. In such a system, the motion of the Cooper pair cannot be described by a diffusion equation, and the microscopic wave character becomes significant. But there have not been any theories to describe a clean superconducting superlattice on a microscopic basis.

We are especially interested in the properties and phenomena related to the spatial variation of the pair potential[23] in the unit period of a periodic nonuniform system, which is an essential feature of superlattices. The one-dimensional Kronig-Penney model[24] can become the starting model of superconductivity in many-band systems. But to make a more realistic model of superconductivity, it is necessary to take into account the three-dimensional motion. The three-dimensional Kronig-Penney model is the simplest but in a certain sense most realistic model of layered materials. Therefore, in the present paper, we aim to extend the one-dimensional Kronig-Penney model[25] to three-dimensional systems by taking into consideration the electron's motion parallel to the layer. This model can be treated analytically based on the rigorous wave function and can describe the essential character of the periodicity, dimensionality, and lack of uniformity of the superconductivity. Moreover, based on the exact Green's function of the Kronig-Penney model, we can establish the theory of superconductivity of many-band systems which is indicated by the Bragg reflection. Since we are interested in the simplest superconducting system, Bardeen-Cooper-Schrieffer (BCS)–type local interelectron coupling[26] is assumed, which is constant in the constant-potential region. The interelectron coupling changes like a step function at the interface, as usually assumed in the theory of the proximity effect (Fig. 1).

The plan of this paper is as follows. In Sec. II the analytical expression of the single-particle Green's function is derived, from which the exact integral kernal of the Gor'kov[27] equation can be calculated. The extension

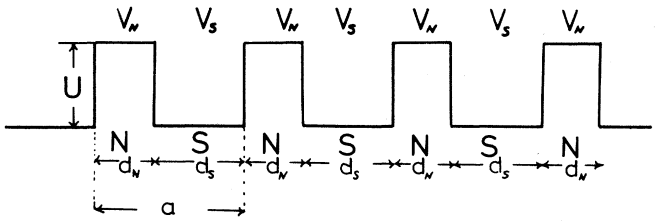

FIG. 1. The picture of the Kronig-Penney model. The quantities d_S and d_N are the width of materials S and N, respectively, and the quantity a is a length of the unit period. The height of the potential is expressed as U. The interelectron potential in each region is expressed as V_S and V_N.

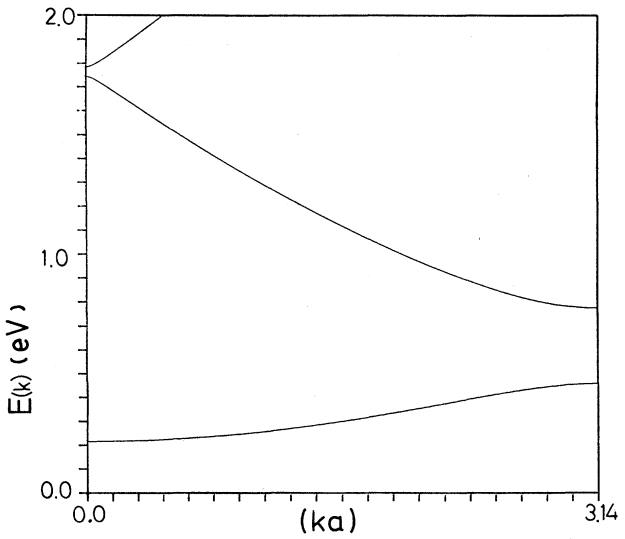

FIG. 2. The energy band structure determined by Eqs. (2.11) and (2.12).

to the three-dimensional system is done by numerical integration. In Sec. III we investigate the superconducting transition temperature in the thin-layered Kronig-Penney model. Our numerical result based on the rigorous equation is compared with the usual estimation of the critical temperature with the use of the density of states. In Sec. IV, the spatial dependence of the pair potential in the Kronig-Penney model is clarified in the thin-layered material and is compared with the result of the one-dimensional Kronig-Penney model. In Sec. V, the critical temperature and spatial dependence of the potential are also investigated, as well as their dependence on the length of the superlattice period.

II. GENERALIZED KRONIG-PENNEY MODEL AND SINGLE-PARTICLE GREEN'S FUNCTION

In this section we obtain the integral kernel for the generalized Kronig-Penney model. The periodic square-well potential assumed in the Kronig-Penney model is shown in Fig. 1. Electrons that travel in the x direction feel this potential change, but this system is uniform in the yz direction. The system is a periodic array of the S and N materials with thickness d_S and d_N, respectively. We only consider the case in which the potential U in the material N is positive, without losing generality. The value of the interelectron coupling $V(x)$ in the S and N region is denoted by V_S and V_N, respectively. We can change the band structure of the system in the normal state by choosing the length d_S, d_N and the height of the potential U. Previous theories of Lawrence and Doniach[5] and Klemm, Luther, and Beasley[4] treat layered materials with the use of a tunneling model. In this model the electron's motion perpendicular to the layer is approximated by a tight-binding model, and parallel to the layer by a free-electron model. Our Kronig-Penney model becomes equivalent to the tunneling model when the potential barrier at the N region is much larger than the Fermi level. If it is wide, the previous theories[4,5] can be reproduced. In this case we consider only the lowest band for the direction perpendicular to the layer. In our theory, the pair potential $\Delta(\mathbf{x})$ depends only on the x coordinate due to the translational invariance for the yz direction, and satisfies the following equation:

$$\begin{aligned}\Delta(\mathbf{x})=\Delta(x)&=V(x)T\sum_{\omega}\int_{-\infty}^{\infty}\int_{-\infty}^{\infty}\int_{-\infty}^{\infty}H_{\omega}(\mathbf{x},\mathbf{x}')\Delta(\mathbf{x}')dx'dy'dz'\\&=V(x)T\sum_{\omega}\int_{-\infty}^{\infty}K_{\omega}(x,x')\Delta(x')dx' .\end{aligned}\tag{2.1}$$

In the preceding equation $H_{\omega}(\mathbf{x},\mathbf{x}')$ is the usual integral kernel of the Gor'kov equation in the three-dimensional system, and $K_{\omega}(x,x')$ is the integrated one in the direction yz, parallel to the layer plane:

$$\begin{aligned}K_{\omega}(x,x')&=\int_{-\infty}^{\infty}\int_{-\infty}^{\infty}H_{\omega}(\mathbf{x},\mathbf{x}')dy'dz'=\int_{-\infty}^{\infty}\int_{-\infty}^{\infty}G_{\omega}(\mathbf{x},\mathbf{x}')G_{-\omega}(\mathbf{x},\mathbf{x}')dy'dz'\\&=1/(2\pi)^2\int_{-\infty}^{\infty}\int_{-\infty}^{\infty}G_{\omega}(x,x',k_y,k_z)G_{-\omega}(x,x',k_y,k_z)dk_ydk_z\\&=m/(2\pi)\int_0^{\infty}G_{\omega}(x,x',\varepsilon)G_{-\omega}(x,x',\varepsilon)d\varepsilon .\end{aligned}\tag{2.2}$$

In Eq. (2.2) $G_{\omega}(\mathbf{x},\mathbf{x}')$ is the single-particle Green's function and can be expressed as

$$G_{\omega}(\mathbf{x},\mathbf{x}')=1/(2\pi)^2\int_{-\infty}^{\infty}\int_{-\infty}^{\infty}G_{\omega}(x,x',k_y,k_z)\exp[ik_y(y-y')+ik_z(z-z')]dk_ydk_z .\tag{2.3}$$

In the last line of Eq (2.2), we introduced $G_\omega(x,x',k_y,k_z)$ by

$$G_\omega(x,x',\varepsilon)=G_\omega(x,x',k_y,k_z)\ , \tag{2.4}$$

since it depends on k_y,k_z by the combined quantity

$$\varepsilon=(k_z^2+k_y^2)/2m\ , \tag{2.5}$$

where m is the effective mass of the electron for the yz direction. At first we obtain the Green's function $G_\omega(x,x',\varepsilon)$, which is given by the Green's function for the motion of the x direction for the effective Fermi level $E_F-\varepsilon$. With use of this Green's function, integral kernel $K_\omega(x,x')$ can be obtained with the integration over ε. The Bloch function $\Psi_k^j(x)$ of the jth energy band with the crystal momentum k along the x direction is given by

$$\Psi_k^j(x)=\Psi_k(x,\alpha_j(k))\ , \tag{2.6}$$

$$\Psi_k(x,\alpha)=\begin{cases}[u_1(\alpha^2-2mU)^{1/2}\sin(\alpha x)-u_2\cos(\alpha x)]/A^{1/2} & (-d_S<x<0)\ ,\\ \{u_1\alpha\sin[(\alpha^2-2mU)^{1/2}x]-u_2\cos[(\alpha^2-2mU)^{1/2}x]\}/A^{1/2} & (0<x<d_N)\ ,\end{cases} \tag{2.7}$$

$$\begin{aligned}u_1&=\cos[(\alpha^2-2mU)^{1/2}d_N]-\cos(\alpha d_S)\exp(ika)\ ,\\ u_2&=\alpha\sin[(\alpha^2-2mU)^{1/2}d_N]+(\alpha^2-2mU)^{1/2}\sin(\alpha d_S)\exp(ika)\ ,\end{aligned} \tag{2.8}$$

$$A=[\partial f(k,\alpha)/\partial\alpha]\{\sin(\alpha d_S)\cos[(\alpha^2-2mU)^{1/2}d_N]+\sin[(\alpha^2-2mU)^{1/2}d_N]\cos(\alpha d_S)[\alpha/(\alpha^2-2mU)^{1/2}]\}\ , \tag{2.9}$$

$$\begin{aligned}f(k,\alpha)=&\cos(ka)-\cos(\alpha d_S)\cos[(\alpha^2-2mU)^{1/2}d_N]\\ &+[(\alpha^2-2mU)^{1/2}/\alpha+\alpha/(\alpha^2-2mU)^{1/2}]\sin(\alpha d_S)\sin[(\alpha^2-2mU)^{1/2}d_N]/2\ .\end{aligned} \tag{2.10}$$

In Eq. (2.6) $\alpha_j(k)$, are the jth solution of the following equations:

$$\alpha^2/2m=\beta^2/2m+U\ , \tag{2.11}$$

$$2\alpha\beta\cos ka=2\alpha\beta\cos(\alpha d_S)\cos(\beta d_n)-(\alpha^2+\beta^2)\sin(\alpha d_S)\sin(\beta d_N)\ . \tag{2.12}$$

The energy of this state measured from the bottom of the potential in S is given by

$$E_j(k)=\alpha_j(k)^2/2m\ , \tag{2.13}$$

and the wave function $\Psi_k^j(x)$ depends on k through the form $\exp(ika)$. The wave function $\Psi_k^j(x)$ is normalized in the unit cell, and an example of its band structure is given in Fig. 2 by the case of $U=0.5$ eV, $d_S=d_N=5.0$ Å. The Green's function can be obtained by

$$G_\omega(x,x',\varepsilon)=\sum_{jk}\Psi_k^{j*}(x)\Psi_k^j(x')/\{i\omega-[E_j(k)-E_F+\varepsilon]\}\ , \tag{2.14}$$

where E_F is the Fermi level and ω is the Matsubara frequency. Thanks to the property of $f(k,\alpha),\partial f(k,\alpha)/\partial\alpha$, this summation can be written by the integral along the path C shown in Fig. 3 for positive ω as

$$G_\omega(x,x',\varepsilon)=(a/2\pi)(1/\pi i)\oint_C\int_{-\pi/a}^{\pi/a}[\partial f(k,\alpha)/\partial\alpha]\Psi_k^*(x,\alpha)\Psi_k(x',\alpha)/[(i\omega-\alpha^2/2m+E_F-\varepsilon)f(k,\alpha)]d\alpha\,dk\ . \tag{2.15}$$

It is easily shown by the translational symmetry of this system that

$$G_\omega(x+na,x'+na,\varepsilon)=G_\omega(x,x',\varepsilon)\quad (n\text{ is integer})\ . \tag{2.16}$$

It is verified as shown in the Appendix that

$$G_\omega(x,x'+na,\varepsilon)=G_\omega(x,x'+na-a,\varepsilon)\exp(iu_+)\quad (n\geq 2)\ , \tag{2.17}$$

$$G_\omega(x,x'-na,\varepsilon)=G_\omega(x,x'-na+a,\varepsilon)\exp(iu_+)\quad (n\geq 2) \tag{2.18}$$

for $|x-x'|\leq a$. In the preceding equations u_+ is defined by

$$\cos(u_+)=\{\cos[\alpha_+d_S+(\alpha_+^2-2mU)^{1/2}d_N]-\cos[\alpha_+d_S-(\alpha_+^2-2mU)^{1/2}d_N]r_+^2\}/(1-r_+^2)\ , \tag{2.19}$$

where a_+,β_+,r_+ are determined by

$$\alpha_+^2/2m=i\omega+E_F-\varepsilon=\beta_+^2/2m+U,\quad r_+=(\alpha_+-\beta_+)/(\alpha_++\beta_+)\ . \tag{2.20}$$

With use of Eq. (2.12), the Green's function for all values of x,x' are obtained. The typical example is written as follows

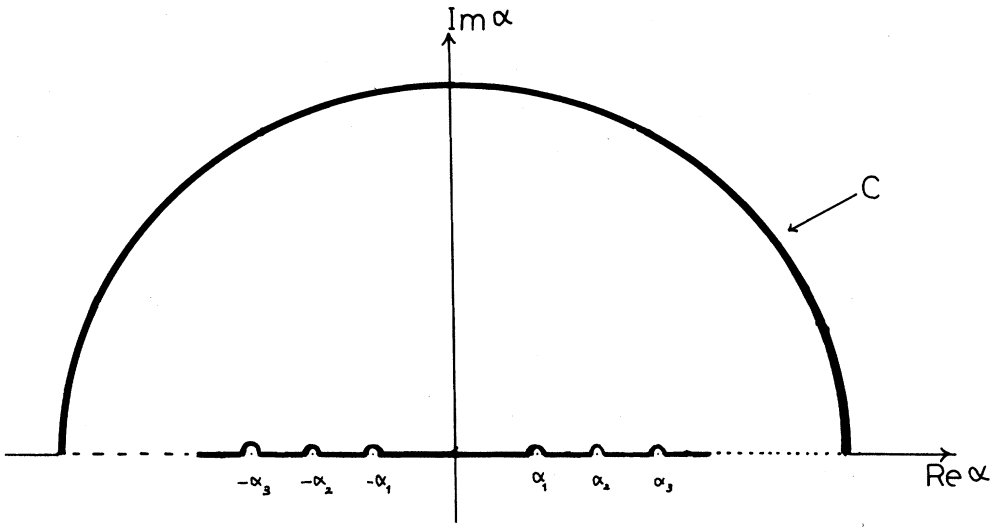

FIG. 3. The integral path in the complex α plane in Eq. (2.15).

for the positive Matsubara frequency:

$$G_\omega(x,x',\varepsilon)=(m/i\alpha_+)[(1-r_+^2)\sin(u_+)]^{-1}$$
$$\times\{\cos[\alpha_+(x-x')[\sin(\alpha_+d_S+\beta_+d_N)-r_+^2\sin(\alpha_+d_S-\beta_+d_N)]+2r_+\cos[\alpha_+(x+x'+d_S)]\sin(\beta_+d_N)$$
$$+i\sin(\alpha_+|x-x'|)\sin(u_+)(1-r_+^2)\}\quad(-d_S<x<0,\ -d_S<x'<0)\ . \tag{2.21}$$

The Green's function for negative ω can be obtained by the same procedure, and the Green's function obtained above can be used for the calculation of the Gor'kov's integral kernel with the use of Eq. (2.2).

III. SUPERCONDUCTING TRANSITION TEMPERATURE OF THE KRONIG-PENNEY MODEL

In this section we consider the superconducting transition temperature T_c of the Kronig-Penney model. In this model, with the use of the periodicity and the property of the single-particle Green's function (see the Appendix), the Gor'kov equation can be transformed as

$$\Delta(x)=V(x)T\sum_\omega\int_{-\infty}^{\infty}K_\omega(x,x')\Delta(x')dx'$$
$$=V(x)T\sum_\omega\int_{-d_S}^{d_N}\int_0^\infty m/(2\pi)^3(K_\omega^0(x,x',\varepsilon)+[K_\omega^0(x,x'+a,\varepsilon)+K_\omega^0(x,x'-a,\varepsilon)]/\{1-\exp[-a/\xi(\varepsilon)]\})$$
$$\times\Delta(x')dx'd\varepsilon\ , \tag{3.1}$$

where the integral kernel $K_\omega^0(x,x',\varepsilon)$ is given by the single-particle Green's function as

$$K_\omega^0(x,x',\varepsilon)=G_\omega(x,x',\varepsilon)G_{-\omega}(x,x',\varepsilon) \tag{3.2}$$

and the decay length of the integral kernel $\xi(\varepsilon)$ is given by Eq. (A13) in the Appendix.

We solve this integral equation numerically by dividing the x axis into fine meshes $\{x_i;\ i=1,2,\ldots,N\}$ and transform it into a secular equation,

$$\sum_j A_{ij}\Delta_j=\Delta_i,\quad \Delta_i=\Delta(x_i)\ , \tag{3.3}$$

$$A_{ij}=(aVT/N)\sum_\omega m/(2\pi)^3\int_0^\infty d\varepsilon(K_\omega(x_i,x_j',\varepsilon)+[K_\omega(x_i,x_j'+a,\varepsilon)+K_\omega(x_i,x_j'-a,\varepsilon)]/\{1-\exp[-a/\xi(\varepsilon)]\})\ . \tag{3.4}$$

The transition temperature is so determined that the maximum eigenvalue of the matrix A_{ij} becomes unity. In this section, for the sake of simplicity, $V(x)$ is assumed to be constant. Due to the ε integral for the calculation of A_{ij}, the numerical calculation becomes much more tedious as compared to the case of the one-dimensional case.[25] In the first place we see the Fermi level (E_F) dependence of the critical temperature for typical cases. In Fig. 4(a) the critical temperature T_c is plotted by asterisks, as the function of E_F for the case of $U=0.5$ eV, $d_S=d_N=5.0$ Å. For the case of $k_{\parallel}=(k_y,k_z)=0$, the dispersion of the lowest and the second band in the k_x direction extends in the region 0.22–0.47 eV, and 0.79–1.75 eV, respectively. In the region between 0.47 and 0.79 eV, the lowest band shows only the two-dimensional dispersion of $k_{\parallel}$, thus the density of state (DOS) is constant in this region.

Usually the critical temperature is estimated by the density of state N with the use of a simple BCS relation as

$$1=T_c\sum_{\omega_n}\pi N/|\omega_n|,\quad T_c\sim\exp(-1/VN)\ . \tag{3.5}$$

It is very interesting whether or not this relation is satisfied even in the system with a nonuniform local DOS. As the reference the critical temperature with the use of Eq. (3.5) is also plotted on the solid line in Fig. 4(a). Our exact numerical calculation shows similar behavior to that shown by the simple estimation of Eq. (3.5). For example, in the energy region where there is no energy dispersion for the k_x direction (0.47–0.79 eV) T_c takes a nearly constant value reflecting the constant value of the DOS. But it can be seen that there exist some differences

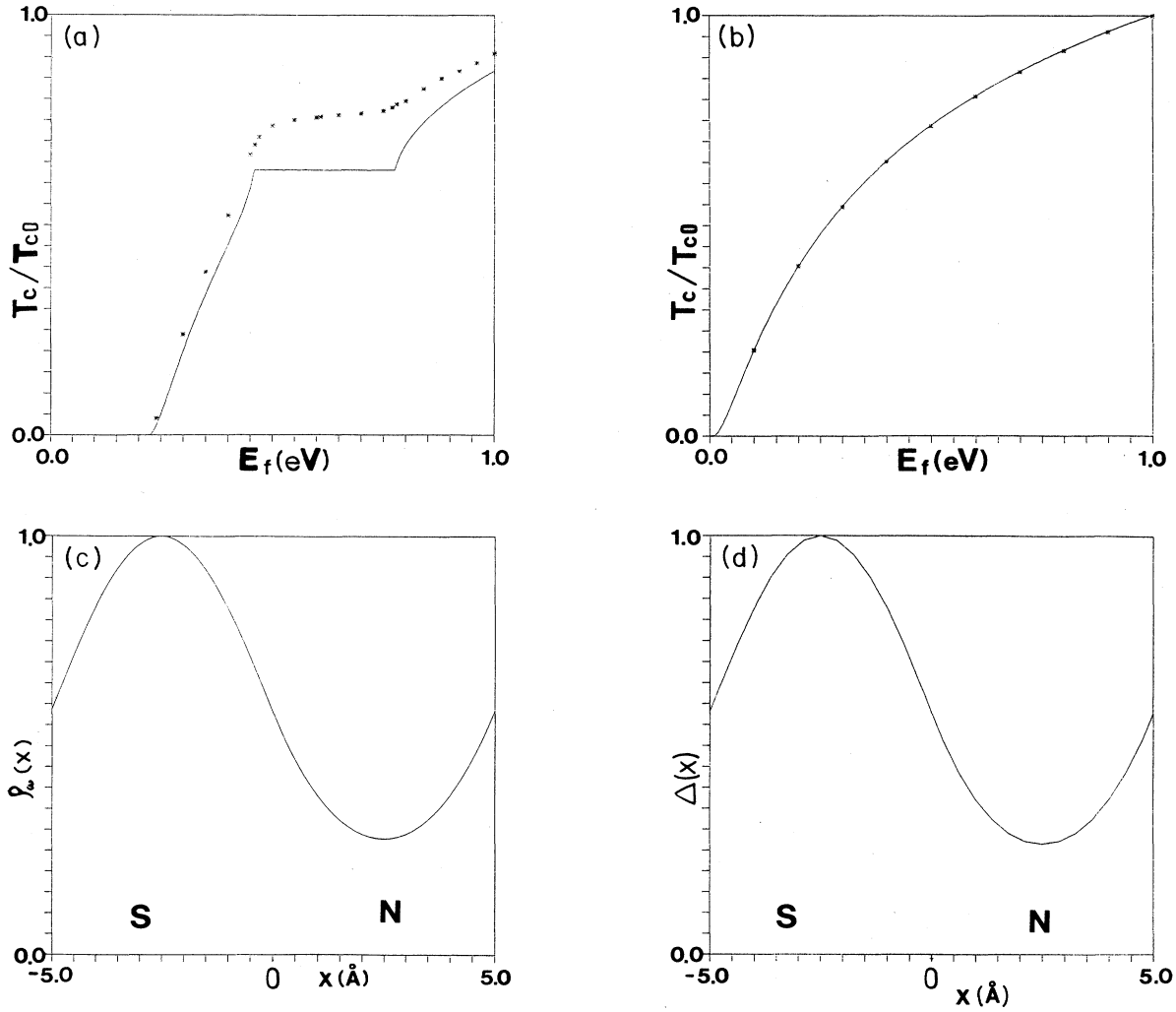

FIG. 4. The critical temperature T_c is plotted by asterisks as the function of E_F for (a) $U=0.5$ (eV), $d_S=d_N=5.0$ Å and (b) $U=0.0$ (eV). As the reference T_c is plotted on the solid line with the use of simple BCS estimation. In this figure T_{c0} is the critical temperature of the system with $U=0.0$ (eV), $E_F=1.0$ (eV). (c) The distribution of the local density of states (LDOS) at T_c is plotted as the function of x for case (a) and $E_F=0.61$ eV. In this figure maximum value is normalized to 1. (d) $\Delta(x)$ is plotted as the function of the same parameter in (c). The maximum value is normalized to 1.

between the two results for the nonuniform system ($U\neq 0$): the curve of the calculated T_c always takes a higher value than expected from Eq. (3.5) and is smooth at the edge of the bands. On the other hand, there are no differences in the case of the uniform system $U=0.0$ eV as shown in Fig. 4(b). To show the nonuniformity of our system, the local DOS, $\rho_\omega(x)$ at Fermi energy $E_F=0.61$ eV for the lowest Matsubara frequency ($\omega=\pi T_c$) at critical temperature,

$$\rho_\omega(x)=-1/\pi \,\mathrm{Im}G_\omega(x,x) \tag{3.6}$$

is plotted in Fig. 4(c). This quantity is almost equal to the usual local DOS at $E_F=0.61$ eV, but includes the lifetime effect at finite temperature of the quasiparticle. Since the Fermi level does not lie at the band edge in this case, the difference between the two is negligible. As shown in Fig. 4(c), $\rho_\omega(x)$ becomes maximum at the center of S and becomes minimum at the center of N. The pair potential $\Delta(x)$ shows similar behavior to $\rho_\omega(x)$ as shown in Fig. 4(d). Based on the spatial variation of $\Delta(x)$ and $\rho_\omega(x)$, why the critical temperature cannot be estimated by the DOS as in Eq. (3.5) is explained. With use of the Gor'kov equation, T_c can be obtained by the solution

$$1\sim T_c \sum_\omega \frac{\pi V}{|\omega_n|}\left[\int_{-d_S}^{d_N}\rho_\omega(x)\Delta(x)dx \Big/ \int_{-d_S}^{d_N}\Delta(x)dx\right]. \tag{3.7}$$

For the case of a uniform system in Fig. 4(b), $\Delta(x)$ is constant and we can estimate T_c correctly with the use of Eq. (3.5). However, in general $\Delta(x)$ does not take constant value, and thus the estimation of T_c by Eq. (3.5) is not valid for the nonuniform system. In the case of Fig. 4(a), $\Delta(x)$ becomes large when the effective DOS $\rho_\omega(x)$ becomes large, as shown in Fig. 4(c) and 4(d). So the transition temperature T_c is enhanced. The enhancement of T_c is generally expected when the periodic variation of the potential is introduced.

IV. PERIODIC SPATIAL VARIATION OF THE PAIR POTENTIAL

In this section, the variation of the pair potential $\Delta(x)$ within the unit period of the Kronig-Penney model is discussed. We will mainly treat the region where the length of the unit period is smaller than the decay length of the integral kernel $\xi(\varepsilon)$. De Gennes considered superconductivity of thin layers in the limit $l\ll d_S, d_N \ll \xi$, where l is the mean-free path of the electron. He concluded the system is equivalent to the uniform system with the effective interelectron coupling $V_{\rm eff}$ and the effective DOS $\rho_{\rm eff}$, satisfying

$$\rho_{\rm eff}V_{\rm eff}=(V_N\rho_N^2 d_N+V_S\rho_S^2 d_S)/(\rho_N d_N+\rho_S d_S)\,, \tag{4.1}$$

where ρ_S and ρ_N are the DOS in the uniform material N and S, respectively. However, if the thickness d_S, d_N are comparable or even smaller than the mean-free path l, the behavior of the Cooper pair in the slab cannot be described by the diffusion motion, since the wave character of the electron prevails. Therefore de Gennes' assumption, on which Eq. (4.1) is based, cannot be valid in such cases. In this section, we study the basic property of the superconductivity of the layered system with $d_S, d_N < 1$. In particular, we investigate the dependence of T_c on the ratio of the coupling constant in the two materials and the spatial variation of the pair potential in the unit cell.

The effective local density of states takes a larger value in the S region as shown in Fig. 4(c). In the following we denote the value of the effective interelectron coupling V used in Sec. III as V_0 ($V_0\sim 0.4$ eV). The critical temperature is shown as the function of V_N/V_0 for $V_S/V_0=1.0$ in Fig. 5(a) and as the function of V_S/V_0 for $V_N/V_0=1.0$ in Fig. 5(b). For the sake of comparison, we also calculated T_c of the same Kronig-Penney system, but

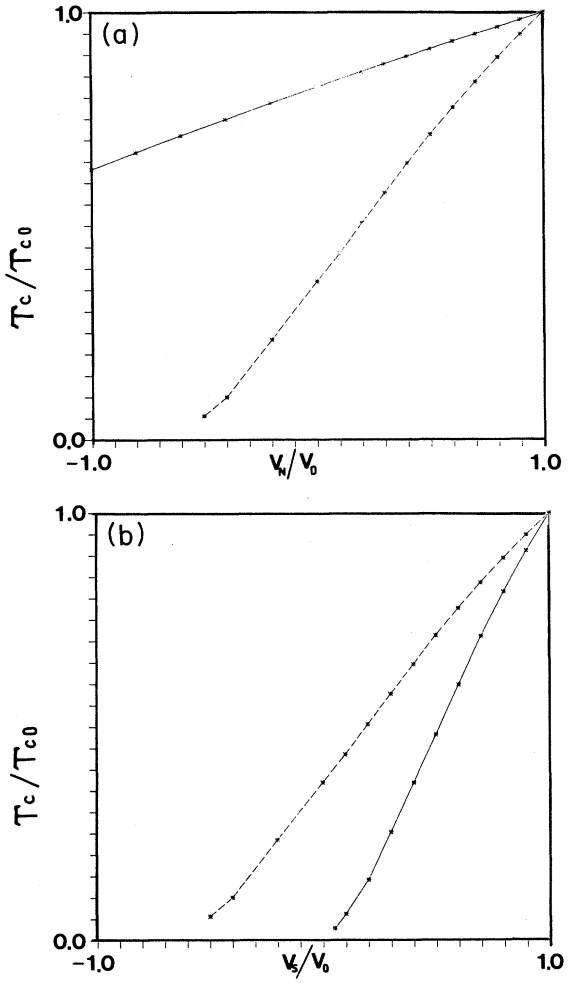

FIG. 5. The critical temperature T_c of the system with $V_S\neq V_N$ (solid line) as the function of (a) V_N/V_0 ($V_0=V_S$) and (b) V_S/V_0 ($V_N=V_0$), for $d_S=d_N=5.0$ Å, $E_F=0.61$ eV, and $U=0.5$ eV. As the reference, the corresponding system with uniform coupling is expressed as a dashed line. In this figure T_{c0} is the value of that of $E_F=0.61$ eV, $V_S=V_N=V_0$, $U=0.5$ eV, $d_S=d_N=5.0$ Å.

with the uniform interelectron coupling constant

$$V_{\text{eff}}=(d_S V_S+d_N V_N)/(d_S+d_N)\ . \tag{4.2}$$

The result is plotted by the dashed line in Fig. 5(a) and 5(b), respectively. In the case of Fig. 5(a) the critical temperature T_c of the system with the uniform coupling V_{eff} is lower than that of the system with $V_S \neq V_N$. On the other hand, in the case of Fig. 5(b), T_c of the former is higher than that of the latter. In this case, the DOS in the region of the larger interelectron coupling is the smaller. Therefore, T_c is suppressed as compared to that in the uniform V_{eff} system [Fig. 5(b)]. It is remarkable that the superconducting state cannot be realized if the coupling V_S becomes negative in the region of the higher local DOS. The characteristics of the results of Fig. 5(a) and 5(b) are summarized as follows. If the local DOS in the N region is smaller than the S region, the decrease in critical temperature as V_N decreases is less extensive. But as indicated in Fig. 5(b), when the local DOS of region S with weaker interelectron coupling is the higher, the suppression of critical temperature due to the decrease of the coupling constant at that region is conspicuous.

The spatial behavior of the pair potential is shown for various V_N in Fig. 6(a) and for various V_S in Fig. 6(b). We cannot know the absolute amplitude of the pair potential, because our treatment is based on the linearized equation for the pair potential. Therefore we normalize the maximum value of the pair potential as unity. In the first place, we see the case where the interelectron coupling constant in S is higher than in N in Fig. 6(a). The values of the parameters are the same as in Fig. 5(a). Even for the case where the common interelectron potential $V_S=V_N$, the pair potential is not constant in the unit cell due to the lack of uniformity. The pair potential becomes large in the region with the higher DOS. As shown in Fig. 6(a), even when pair breaking occurs in N, i.e., V_N becomes negative, the behavior of the pair potential in the region S hardly changes. On the other hand, the pair potential in N changes drastically depending on V_N. It can be shown analytically by Eq. (3.1) that $\Delta(x)$ satisfies the following relation:

$$\Delta(x=0_+)/\Delta(x=0_-)=V_N/V_S\ , \tag{4.3}$$

which is also verified by the numerical calculation. Next we discuss the case where the effective interelectron potential in S becomes smaller than that of N as shown in Fig. 6(b). The same values of the parameters are used as in Fig. 5(b). The pair potential shows very different behavior from that in Fig. 6(a). When V_S/V_0 decreases from unity to 0.8, the normalized pair potential increases in the region N while it does not change significantly in the region S. When V_S/V_0 decreases further below 0.5, the pair potential in the region S starts to diminish. The pair potential becomes maximum at the S-N interface.

When two conditions favoring the superconductivity, i.e., the higher DOS and the stronger interelectron coupling, are not satisfied simultaneously in the same material side, the competition of the two effects occurs. This seems the reason why the pair potential concentrates to the S-N interface in such cases as shown in the above numerical results. If either side of the material, S or N, satisfies both of the conditions, the pair potential takes a maximum value at the middle of the layer of that material. However, when only one of the conditions is satisfied, the pair potential can take a maximum value at the boundary. We have already found these features in the simple one-dimensional Kronig-Penney model.[25] In the present work, it is verified that this feature is not changed in three-dimensional thin superlattice system.

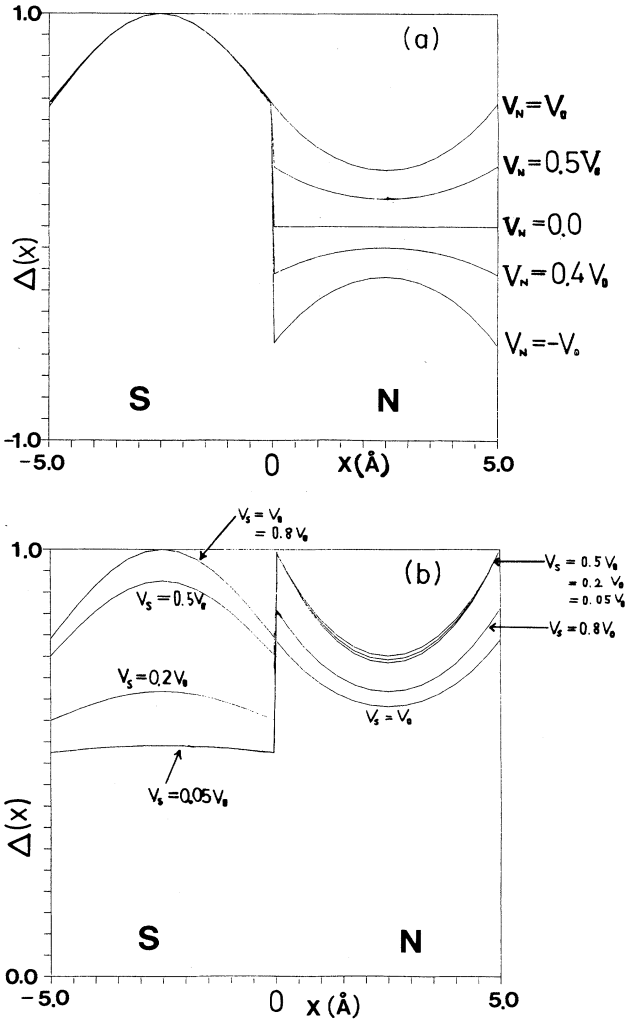

FIG. 6. The spatial dependence of pair potential $\Delta(x)$ is plotted for various V_N/V_0 ($V_S=V_0$) in (a), and for V_S/V_0 ($V_N=V_0$) in (b). The maximum value of $\Delta(x)$ is normalized to 1.0.

V. DEPENDENCE OF THE SUPERCONDUCTING PROPERTY ON THE LENGTH OF THE UNIT PERIOD OF THE SUPERLATTICE

In this section, we consider the case where the unit period length is increased to exceed the decay length $\xi(\varepsilon)$. In such a case numerical calculation becomes tedious because the number of meshes of numerical integrals

over the unit periods increases. As in the previous sections, it is assumed that the DOS in the S region is larger than in the N region. We consider the typical three cases,

(a) $U=0.5$ eV, $E_F=0.7$ eV (metal-metal junction),

(b) $U=0.5$ eV, $E_F=0.5$ eV (metal-semiconductor junction),

(c) $U=1.0$ eV, $E_F=0.5$ eV (metal insulator junction).

For (b) and (c) there are no conducting electrons in the N region. For the first step we take the interelectron potential $V(x)$ as constant ($V_S=V_N$) and treat only the case of $d_S=d_N$. It should be remarked that in (b) and (c), since there is no conducting electron, the isolated N system cannot become a superconductor as the system of N alone. But in (a), N can become a superconductor that has a lower critical temperature than S. The critical temperature T_c obtained by numerical calculations as described in Sec. III is plotted by the solid line in Fig. 7 as the function of $a=d_S+d_N$ for the three cases (a), (b), and (c). For the case of a very thin limit,

$$a|\alpha_+|\ll 1, \quad a|\beta_+|\ll 1, \tag{5.1}$$

the local DOS becomes constant in the unit period, and proportional to the square root of the average kinetic energy at the Fermi level, $(E_F-U/2)^{1/2}$. So the character of superconductivity is described by the uniform system with the averaged potential. In case (c), $E_F-U/2$ becomes zero and the DOS of the averaged system at the Fermi level becomes zero, so that the critical temperature vanishes.

The transition temperature approaches that of the pure S system in the large-a limit. With a decrease of a, T_c is gradually lowered for cases (a) and (b). This effect is explained by the proximity effect which reduces T_c of the thin-film superconductor. The thinner the slab, the more T_c is reduced. The lowering of T_c is less significant in (c), as compared to case (a) or (b). This can be understood easily, since the barrier of the N region suppresses the proximity effect. When the length of the period is shortened to the same order as the decay length $\xi(\varepsilon)$, an oscillatory behavior of T_c sets in. This is caused by the oscillatory change of the DOS at E_F due to the band effect. The amplitude of the oscillation is much larger in case (c) than in case (a), since the corresponding energy gap is larger in the former case reflecting the higher potential barrier. When the period of the superlattice becomes very short as given by the condition (5.1), T_c again approaches some constant value. This is because the superlattice system becomes a uniform system in which the local DOS and the pair potential take constant value.

In the following, we describe the spatial dependence of the pair potential. For very small a satisfying Eq. (5.1), the pair potential takes a constant value in all cases [(a)–(c)]. When a is increased to the order of 10 Å, the pair potential shows a sinusoidal behavior taking the maximum value at the middle of S, and becomes

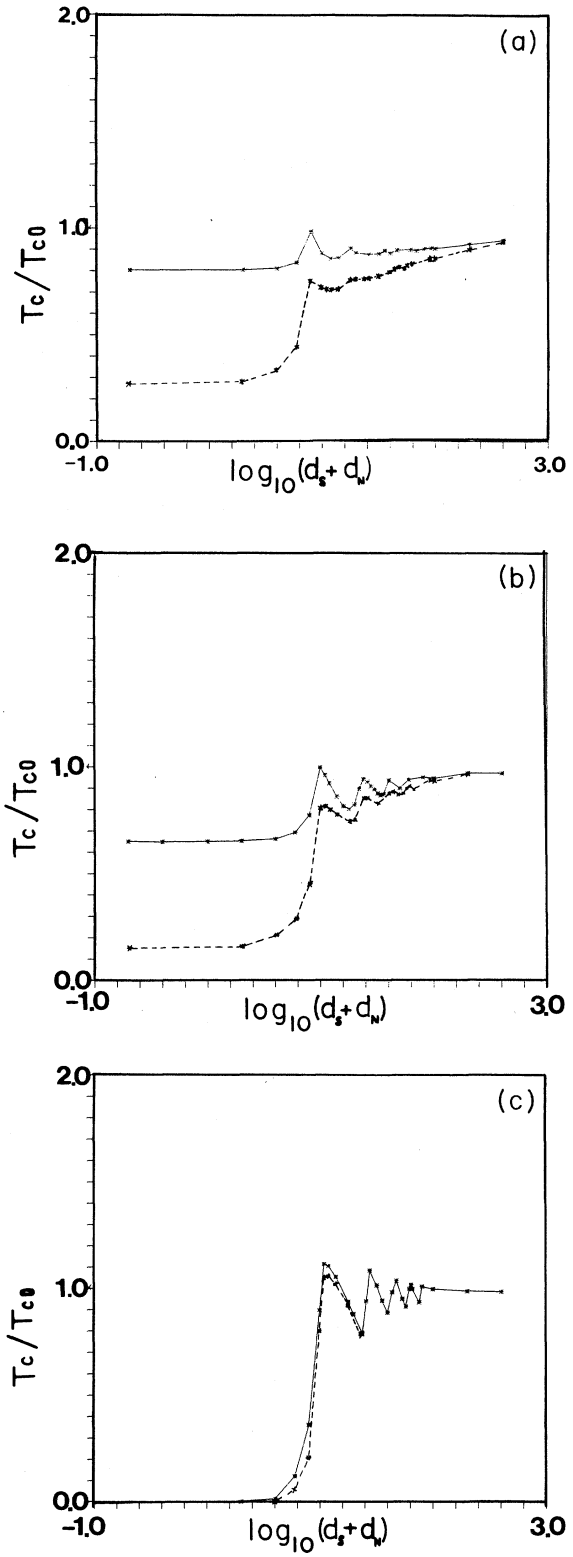

FIG. 7. The critical temperature is plotted as the function of the unit period a (Å)$=d_S+d_N$. This value is normalized by the value of that of S alone, T_{c0}. The solid line is $V_N=V_S$ and the dotted line is $V_N=0$ for fixed V_S. (a) $U=0.5$ eV, $E_F=0.7$ eV; (b) $U=0.5$ eV, $E_F=0.5$ eV; (c) $U=1.0$ eV, $E_F=0.5$ eV.

minimum at the middle of N. This is a common feature for all cases. The typical behavior in this region is shown in Fig. 4(d). With further increase of a, some difference of the spatial behavior of $\Delta(x)$ appears between the three cases. In Fig. 8 the case of $a=40$ Å is shown. In Fig. 8 (a), the pair potential oscillates in the S and N regions for several times. A characteristic oscillation begins to appear near the interface, which is a behavior reminiscent of the Friedel oscillation. With decreasing E_F as in Fig. 8(b), the oscillation in the N region vanishes and $\Delta(x)$ decays monotonously towards the inner N region. As the barrier height U is increased further, $\Delta(x)$ concentrates more in the S region and is very much reduced in the$N$ region as shown in Fig. 8(c). This is due to the fact that the wave function cannot penetrate deep to the center of this region because of the high barrier in the N region.

The behavior of pair potential $\Delta(x)$ for larger values of a is shown in Figs. 9(a)–9(c). In such regions the critical temperature approaches the bulk value of S, as mentioned before. In such regions the common feature for all cases from (a) through (c) is that the pair potential $\Delta(x)$ becomes maximum near the interface and there appear fine oscillations in the S side. With coarse graining of this oscillation, we can extract macroscopic behavior $\Delta(x)$ which is treated in the usual theory of the proximity effect. In case (a), this coarse grained value becomes maximum at the middle of S and decreases slowly towards the interface. But on the other hand, in cases (b) and (c), the coarse grained value of Δ becomes constant in the S region. Next we see the behavior of the pair potential in the region of N. It becomes small going deeper into the N region . The decay length of the pair potential is remarkably different whether conductive electrons exist in the N region or not. The effective chemical potential in N is (a) 0.2 eV, (b) 0.0 eV, and (c) -0.5 eV, respectively. In Figs. 9(b) and 9(c), $\Delta(x)$ hardly penetrates into the N region and the decay length of the integral kernel in N becomes of atomic order.

Further we show how the above property changes when V_N becomes small, for example, when V_N becomes zero. In Figs. 7(a)–7(c) the critical temperature T_c is plotted by the dotted line for the case of $V_N=0$. It is clear that the case of $V_N=0$ shows a lower critical temperature as compared to the case of $V_S=V_N$. For the very thin limit, the local DOS becomes constant as written previously. But the interelectron coupling becomes nonuniform. Because the local DOS is constant, the transition temperature T_c is reduced to the value corresponding to the system with the averaged interelectron potential $V_S/2$. The reduction from that of the uniform interaction case $V_S=V_N$ is most significant for the thin limit.

The transition temperature approaches that of the pure S system in the large-a limit as in that for $V_S=V_N$. With a decrease of a, T_c is gradually lowered for cases (a) and (b). This tendency is more significant than that of $V_S=V_N$. In case (c), as compared to cases (a) or (b) the difference between $V_S\neq V_N$ and $V_S=V_N$ is not so large. This can be understood easily, since the barrier of the N region suppresses the proximity effect and the interelectron potential in N hardly influences the property of su-

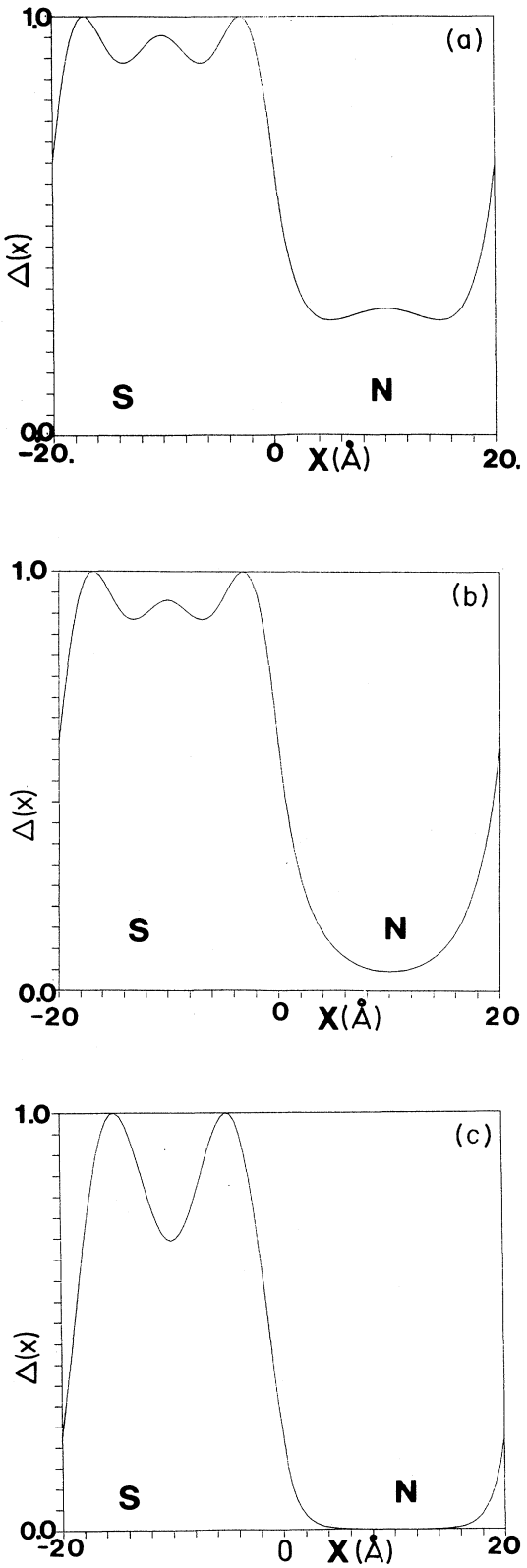

FIG. 8. The spatial dependence of the pair potential is plotted for $d_S=d_N=20.0$ Å. (a) $U=0.5$ eV, $E_F=0.7$ eV; (b) $U=0.5$ eV, $E_F=0.5$ eV; (c) $U=1.0$ eV, $E_F=0.5$ eV.

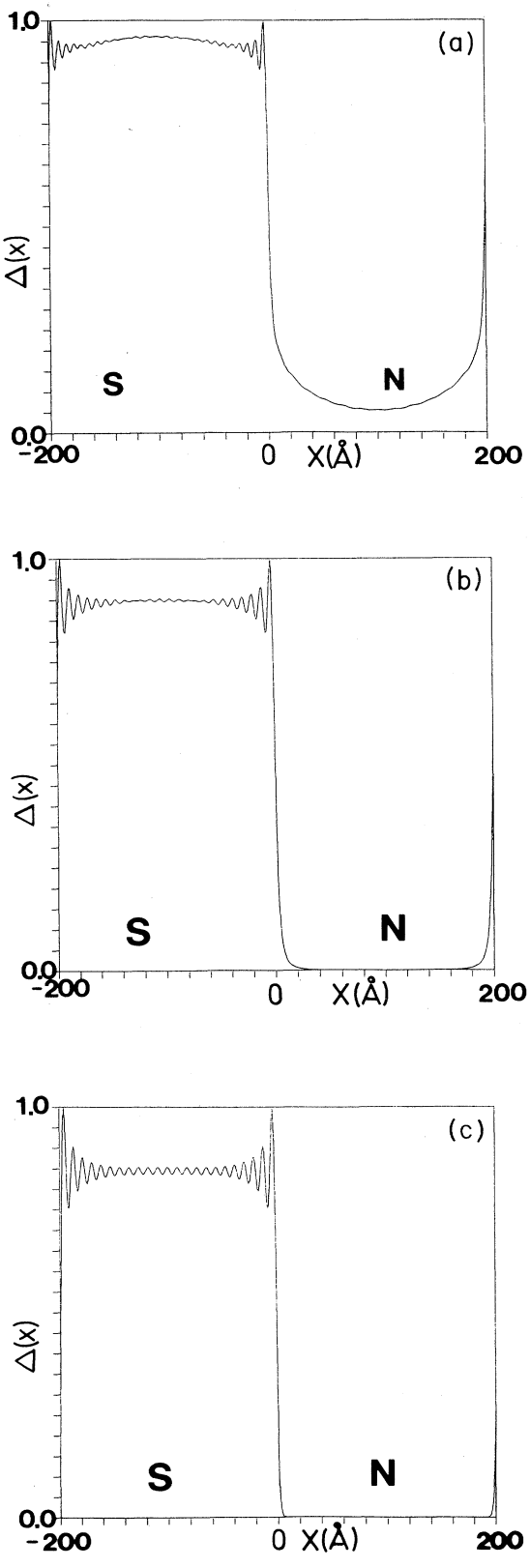

FIG. 9. The spatial dependence of the pair potential is plotted for $d_S = d_N = 200.0$ Å. (a) $U = 0.5$ eV $E_F = 0.7$ eV; (b) $U = 0.5$ eV, $E_F = 0.5$ eV; (c) $U = 1.0$ eV, $E_F = 0.5$ eV.

perconductivity except for the case of very small a. When the length of the period is shortened to the same order as the decay length $\xi(\varepsilon)$, an oscillatory behavior of T_c sets in as in the case of $V_S = V_N$. It can be concluded that the value of V_N affects very significantly cases (a) and (b), especially for small a, but in case (c) this effect is very small. Whether the N region is a barrier or not is the most important factor in determining the strength of the proximity effect. But regardless of the value of V_N the oscillatory behavior of the critical temperature can be observed due to the band effect.

VI. CONCLUSION

In this paper, we have developed a theory of superconductivity in the Kronig-Penney model for the layered materials. As the model is three-dimensional, this is the simplest realistic theory of the layered material and superlattices. So the results obtained here based on the exact Green's function represent characteristics inherent in layered superconductivity. With use of this model, we have clarified several new features of the nonuniform superconductivity.

(1) The critical temperature in the nonuniform system cannot be determined by the simple DOS, but by the DOS weighted by the spatially dependent pair potential. Therefore it cannot be determined unless we solve the Gor'kov equation.

(2) For thin superconducting superlattices, we clarified the interplay of two factors favoring the superconducting state, the high DOS, and the large interelectron potential. When in either side of material, these two factors are satisfied at the same time, the pair potential becomes maximum in this side. But when these two conditions are not satisfied simultaneously a competition of these two effects occurs, and the pair potential can take the maximum value at the interface.

(3) The critical temperature shows characteristic behavior as the function of the length of unit period a. The critical temperature oscillates as the function of a, the origin of which is ascribed to the oscillation of the DOS with the lattice constant a. The amplitude of oscillation is much reduced when a is large. The spatial dependence of the pair potential in the unit period changes drastically with the length a. With the increase of a, macroscopic behavior of the proximity effect of the S-N junction emerges as the coarse grained part of the pair potential, on which microscopic oscillation overlaps.

We have planned to publish elsewhere our calculations of the superconductivity of the same model with the extension of the phenomenological theory by de Gennes. In this treatment, the superconducting transition temperature shows only monotonic behavior. Comparing the result based on the exact microscopic theory of the present paper with such a theory based on de Gennes' treatment, it is confirmed that the picture of the previous theory of proximity effect is obtained by coarse graining of the microscopic oscillation of $\Delta(x)$. This oscillation, however, becomes dominant when a becomes small, and governs superconducting properties of thin superlattice. In the present theory we discovered a new type of oscillation of

the critical temperature as a changes which originates from the microscopic nonuniform electronic property due to the Bragg reflection. In the previous treatment of de Gennes, the microscopic electronic property cannot be taken completely, and this oscillation cannot be expected. This oscillation should be examined in the clean superconducting superlattice in the near future. Although the interelectron potential is assumed phenomenologically at this stage, our theory is interesting in the scope of microfabrication.

We discussed many aspects of superconductivity with the numerical solution of the Gor'kov equation obtained by the Green's function of Kronig-Penney model. There remain many problems to be addressed in the next stage: To make a more realistic theory of superconductivity, the assumed interelectron potential must be determined in a more realistic way from the microscopic level. Our theory must be extended to the region below critical temperature and the absolute amplitude of the pair potential should be discussed.

ACKNOWLEDGMENTS

The numerical calculations were performed by the HITAC S820 computer system at the Computor Center of the University of Tokyo, and the Computor Center of the Institute for the Molecular Science. This work was supported by a Grant-in-Aid from the Minstry of Education, Science and Culture, Japan.

APPENDIX

In this appendix, we derive Eqs. (2.17)–(2.21). We take the summation over index j by transforming a discrete summation to an integral along the path shown in Fig. 3. Evaluating this integral, we obtain the following expressions:

$$G_\omega(x,x'+a,\varepsilon)=(a/2\pi)\int_{-\pi/a}^{\pi/a} dk\, F_\omega^+(x,x',\exp(ika))[\sin^2(ka/2)-\sin^2(u_+/2)]^{-1}\,, \tag{A1}$$

$$G_\omega(x,x'+na,\varepsilon)=(a/2\pi)\int_{-\pi/a}^{\pi/a} dk\, F_\omega^+(x,x',\exp(ika))\exp[ik(n-1)a][\sin^2(ka/2)-\sin^2(u_+/2)]^{-1}\,, \tag{A2}$$

$$G_{-\omega}(x,x'-a,\varepsilon)=(a/2\pi)\int_{-\pi a}^{\pi/a} dk\, F_\omega^-(x,x',\exp(ika))[\sin^2(ka/2)-\sin^2(u_-/2)]^{-1}\,, \tag{A3}$$

$$G_{-\omega}(x,x'-na,\varepsilon)=(a/2\pi)\int_{-\pi/a}^{\pi/a} dk\, F_\omega^-(x,x',\exp(ika))\exp[ik(n-1)a][\sin^2(ka/2)-\sin^2(u_-/2)]^{-1}\,. \tag{A4}$$

In the preceding equations, u_+ and u_- are given by

$$\cos(u_+)=\{\cos[\alpha_+ d_S+(\alpha_+^2-2mU)^{1/2}d_N]-\cos[\alpha_+ d_S-(\alpha_+^2-2mU)^{1/2}d_N]r_+^2\}/(1-r_+^2)$$
$$=\cos^*(u_-)\,, \tag{A5}$$

$$|\exp(iu_+)|<1\,, \tag{A6}$$

$$|\exp(iu_-)|<1\,, \tag{A7}$$

$$\alpha_+^2/2m=i\omega+E_F-\varepsilon=\beta_+^2/2m+U\,, \tag{A8}$$

and ω is the positive Matsubara frequency.

The quantities $F_\omega^+(x,x'\exp(ika))$ and $F_\omega^-(x,x',\exp(ika))$ have no singularity as the function of k and the integrals in Eq. (A1)–(A4) can be estimated by the residue of

$$[\sin^2(ka/2)-\sin^2(u_+/2)]^{-1}\,.$$

Finally the following equations are obtained:

$$G_\omega(x,x'+na,\varepsilon)=G_\omega(x,x'+a,\varepsilon)\exp[iu_+(n-1)a]\,, \tag{A9}$$

$$G_\omega(x,x'-na,\varepsilon)=G_\omega(x,x'-a,\varepsilon)\exp[iu_+(n-1)a]\,. \tag{A10}$$

We can obtain the same relation for $G_{-\omega}(x,x'-a,\varepsilon)$ and $G_{-\omega}(x,x'+a,\varepsilon)$ with the use of the preceding discussions, and the following relations for the integral kernel Eq. (3.2) are obtained:

$$K_\omega^0(x,x'+na,\varepsilon)=K_\omega^0(x,x'+a,\varepsilon)\exp[-a(n-1)/\xi]\,, \tag{A11}$$

$$K_\omega^0(x,x'-na,\varepsilon)=K_\omega^0(x,x'-a,\varepsilon)\exp[-a(n-1)/\xi]\,, \tag{A12}$$

$$\xi(\varepsilon)=a/2\,\mathrm{Im}(u_+)\,, \tag{A13}$$

for positive ω, and

$$\xi(\epsilon)=a/2\,\mathrm{Im}(u_-)\,, \tag{A14}$$

for negative ω.

[1] J. Bednorz and K. A. Müller, Z. Phys. B **64**, 189 (1986).

[2] T. Nishino, E. Yamada, and U. Kawabe, *ibid.* **33**, 2042 (1986); T. Nishino, U. Kawabe, and E. Yamada, *ibid.* **34**, 4857 (1986).

[3] H. Takayanagi and T. Kawakami, Phys. Rev. Lett. **54**, 2449 (1985); T. Kawakami and H. Takayanagi, Appl. Phys. Lett. **46**, 92 (1985).

[4] R. A. Klemm, A. Luther, and M. R. Beasley, Phys. Rev. B **12**, 877 (1975).

[5]W. Lawrence and S. Doniach, *Proceedings of the 12th International Conference on Low Temperature Physics,* edited by E. Kanda (Academic Press of Japan, Tokyo, 1971), p. 361.
[6]S. T. Ruggiero, T. W. Barbee, and M. R. Beasley, Jr., Phys. Rev. Lett. **45**, 1299 (1980).
[7]H. Homma, C. S. L. Chun, G. G. Zheng, and I. K. Schuller, Phys. Rev. B **33**, 3562 (1986).
[8]K. Kanoda, H. Mazaki, T. Yamada, N. Hosoito, and T. Shinjo, Phys. Rev. B **33**, 2052 (1986).
[9]S. Takahashi and M. Tachiki, Phys. Rev. B **33**, 4620 (1986); **34**, 3162 (1986).
[10]G. Deutscher, O. Entin-Wohlman, Phys. Rev. B **17**, 1249 (1978).
[11]K. R. Biagi, V. G. Kogan, and J. R. Clem, Phys. Rev. B **32**, 7165 (1985).
[12]J. Clarke, Proc. R. Soc. London, Ser. A **308**, 447 (1969).
[13]P. G. de Gennes, in *Superconductivity of Metals and Alloys* (Benjamin, New York, 1969).
[14]G. Deutscher, P. G. de Gennes, in *Superconductivity,* edited by R. D. Parks (Marcel Dekker, New York, 1969), p. 1005.
[15]P. G. de Gennes, Rev. Mod. Phys. **36**, 225 (1964).
[16]W. L. McMillan, Phys. Rev. **175**, 537 (1968); **175**, 559 (1968).
[17]O. Entin-Wohlman and T. Bar-Sagi, Phys. Rev. B **18**, 3174 (1978).
[18]G. B. Arnold, Phys. Rev. B **18**, 1076 (1978); **17**, 3576 (1978); Phys. Rep. **91**, 31 (1982).
[19]R. L. Kobes and J. P. Whitehead, Phys. Rev. B **36**, 121 (1987).
[20]B. D. Josephson, Phys. Lett. **1**, 251 (1962).
[21]V. Ambegaokar and A. Baratoff, Phys. Rev. Lett. **10**, 486 (1963); **11**, 104 (1963).
[22]I. O. Kulik and A. N. Omely'anchuk, Fiz. Nizk. Temp. **3**, 945 (1977) [Sov. J. Low. Temp. Phys. **3**, 419 (1980)].
[23]Y. Tanaka and M. Tsukada, Phys. Rev. B **37**, 5087 (1988); **37**, 5095 (1988); Solid State Commun. **65**, 287 (1988).
[24]R. de L. Kronig and W. G. Penney, Proc. R. Soc. London, Ser. A **130**, 499 (1931).
[25]Y. Tanaka and M. Tsukada, Solid State Commun. **69**, 195 (1989); **69**, 491 (1989).
[26]J. Bardeen, L. N. Cooper, and J. R. Schriefer, Phys. Rev. **108**, 1175 (1957).
[27]L. P. Gor'kov, Zh. Eksp. Teor. Fiz. **37**, 1407 (1959) [Soviet Phys.—JETP **10**, 998 (1960)].